

Ambiguity of the final state interaction for neutral-current neutrino-nucleus scattering in the quasielastic region

K. S. Kim,^{1,*} Myung-Ki Cheoun,² and W. Y. So³¹*School of Liberal Arts and Science, Korea Aerospace University, Koyang 412-791, Korea*²*Department of Physics, Soongsil University, Seoul 156-743, Korea*³*Department of Radiological Science, Kangwon National University, Samcheok 245-711, Korea*

(Received 21 December 2012; revised manuscript received 16 September 2013; published 23 October 2013)

We investigate the effect of final state interaction (FSI) on the neutrino (antineutrino) scattering via neutral current from a ^{12}C target in the quasielastic region within the framework of a relativistic single-particle model. Three different descriptions of the FSI, which are a relativistic mean field, a complex optical potential, and its real potential, are taken into account for two incident neutrino energies of 500 MeV and 1 GeV. The effects of the FSI are studied not only on the differential cross sections but also on each longitudinal, transverse, and transverse interference cross section. We found that the FSI description may play a vital role for the estimation of those cross sections, and the FSI effects on each response cross section may differ from those on the differential cross section. However, the asymmetry between neutrino and antineutrino scattering cross sections turns out to be nearly independent of the FSI descriptions. Finally, possible FSI effects on the MiniBooNE data are studied in detail.

DOI: [10.1103/PhysRevC.88.044615](https://doi.org/10.1103/PhysRevC.88.044615)

PACS number(s): 25.30.Pt, 24.10.Jv

I. INTRODUCTION

With recent developments in neutrino beam facilities, neutrino-nucleus (ν - A) scattering is emerging as a feasible nuclear reaction to be widely applied in various fields of physics such as astrophysics, cosmology, particle physics, and nuclear physics. In particular, in nuclear physics, ν - A scattering becomes one of the useful tools to study weak interaction, such as strangeness, axial form factor of nucleons [1], and so on. But on the interpretation of the ν - A scattering data in the quasielastic (QE) region, the ambiguity coming from the final state interaction (FSI) between the outgoing knocked-out nucleons and the residual nucleus, which is one of the most important ingredients in the scattering at the intermediate energy range, should be pinned down for further study of the roles of neutrino interaction with nuclei or nuclear matter in other fields.

Recently, since the first measurement of muon neutrino (ν_μ) scattering off a CH_2 target via the neutral current (NC) at BNL [2] and charged-current (CC) reactions at MiniBooNE [3], several neutrino oscillation experiments have been performed at long-baseline facilities such as T2K and MINOS [4,5]. They found the indication for the nonvanishing unknown mixing angle $\sin^2 2\theta_{13}$ in a three-flavor neutrino oscillation, which was confirmed at Double Chooze [6] and measured afterwards by reactor neutrino experiments [7,8]. But in this work, we limit the ν - A scattering in the QE scattering region at T2K, MiniBooNE, and Minerva. In particular, we focus on a recent MiniBooNE experiment [9], which measured the flux-averaged neutral-current (NC) elastic cross sections on CH_2 and the experimental data are explained by nonstandard values of the axial mass and the strange axial form factor at $Q^2 = 0$, $M_A = 1.39$ GeV, and $g_A^s = 0.08$.

A lot of theoretical works [10–16] for the ν - A scattering have been done. Amaro *et al.* [10] tried to explain the muon neutrino cross section [3] by using the superscaling approach (SuSA) but that failed, so they added the meson exchange current in the two-particle two-hole (2p-2h) sector. Nevertheless, the results might not describe the data well. Various theoretical approaches [12–14] to explain the MiniBooNE data investigated the effect of the 2p-2h based on the random phase approximation (RPA) in the QE and the Δ resonance regions [14].

For example, Butkevich and Perevalov [14] calculated the ν - ^{12}C scattering via the NC and found that the strange axial form factor at $Q^2 = 0$ is $g_A^s = -0.11 \pm 0.36$ to fit the MiniBooNE data. In Ref. [15], the axial strangeness does not affect the cross section but the ratio of the cross sections of protons and neutrons is sensitive to the strange quark contribution. Recently, the NC cross section in the QE region was calculated within two models: one was the SuSA approach and the other was relativistic mean field theory (RMF) [16]. It turns out that they need different values for the nucleon axial mass and the strange axial form factor for each model calculation.

In addition, for the FSI in the ν - A scattering, two different methods were exploited: the complex optical potential [17] and the relativistic multiple scattering Glauber approximation (RMSGGA) developed by the Ghent group [18]. Martinez *et al.* [19] compared the two relativistic models to treat the FSI: a relativistic distorted wave impulse approximation (DWIA) and the RMSGGA. The authors addressed that two models provide identical results. Within the framework of a relativistic Green's function [17], the FSI of the knocked-out nucleon in the CC reaction was taken into account through a complex optical potential, but there is no loss of flux. As another approach for the FSI, Meucci *et al.* [20] adopted a relativistic optical potential and discussed the importance of the FSI on the extraction of the strange quark contents in the

*kyungsik@kau.ac.kr

NC reaction. For the interaction beyond 1p-1h approximation, the neutrino scattering was calculated by using a Monte Carlo simulation method within the RPA [21] and then the sensitivity of the final nucleons was found to be important for the ratio of protons to neutrons. The Giessen group [22] has taken the inelastic channels into account for the FSI in the NC reaction by means of the Giessen Boltzmann-Uehling-Uhlenbeck (GiBUU) model and has claimed the contribution of Δ is comparable to that of the QE scattering. In our previous papers, we showed that the cross sections of the NC [23] and the CC reactions [24] were reduced about 50%, maximally, due to the FSI, by using the nuclear model generated by the Ohio group [25,26].

The effect of the FSI on electron scattering has been extensively discussed for the last two decades, but in ν - A scattering in the QE region, where the inelastic processes like the Δ resonance are excluded, it is still worthwhile to study the FSI precisely for more comprehension of the weak interaction with nuclei because the FSI in neutrino NC scattering becomes more complicated due to nondetection of final leptons and nonfixed incident neutrino energy. Therefore, the main physical quantities in the experiment are the cross sections averaged by the presumed incident neutrino flux in terms of squared four-momentum transfer. Nevertheless, the FSI deduced from electron scattering is still a useful guideline.

In this work, we extend our previous results [23,24], which calculated ν scattering via the NC [23] and the CC [24] with an optical potential deduced from electron scattering. To include the FSI, we use three different approaches for the wave function of the final nucleons affected by the FSI. The first approach is wave functions obtained from a relativistic phenomenological optical potential [27]. The second one is wave functions extracted from only a real part of the optical potential with the assumption of no loss of flux. The last one is the wave functions generated by using the same potential of the bound nucleons, called the RMF. This RMF model guarantees the current conservation and gauge invariance. The wave functions of the bound nucleons are generated by a single-particle model in the presence of the strong vector and scalar potentials based on the σ - ω model [28]. Incident ν and antineutrino ($\bar{\nu}$) energies are focused on a range between 0.5 and 1.0 GeV. But for the flux-averaged cross section, we increase the energy up to 3 GeV by following the MiniBooNE data.

Furthermore, we investigate the FSI effects on knocked-out protons (or neutrons) to be exclusively measured in inclusive ν - A scattering. Because the FSI effect was not studied on each response cross section, such as longitudinal and transverse cross sections, we study the FSI effect on response functions because they may be feasible observables in future scattering experiments.

In Sec. II, the formalism is briefly introduced. Our numerical results are presented in Sec. III with detailed discussions on the relevant cross sections and the MiniBooNE data. Finally, the summary and conclusion are given in Sec. IV.

II. FORMALISM

To calculate the $\nu(\bar{\nu})$ - A scattering, we choose the nucleus fixed frame where the target nucleus is seated at the origin of

the coordinate system. The four-momenta of the incident and outgoing neutrinos (antineutrinos) are labeled $p_i^\mu = (E_i, \mathbf{p}_i)$ and $p_f^\mu = (E_f, \mathbf{p}_f)$. $p_A^\mu = (E_A, \mathbf{p}_A)$, $p_{A-1}^\mu = (E_{A-1}, \mathbf{p}_{A-1})$, and $p^\mu = (E_p, \mathbf{p})$ represent the four-momenta of the target nucleus, the residual nucleus, and the knocked-out nucleon, respectively. In the laboratory frame, the inclusive cross section is given by the contraction between the lepton and hadron tensor [19]:

$$\frac{d\sigma}{dT_p} = 4\pi^2 \frac{M_N M_{A-1}}{(2\pi)^3 M_A} \int \sin\theta_l d\theta_l \times \int \sin\theta_p d\theta_p p f_{\text{rec}}^{-1} \sigma_M^Z [v_L R_L + v_T R_T + h v_T' R_T'], \quad (2)$$

where θ_l denotes the scattering angle of the lepton, θ_p is the polar angle of the knocked-out nucleons, and $h = -1$ ($h = +1$) corresponds to the helicity of the incident ν ($\bar{\nu}$). R_L , R_T , and R_T' are the response longitudinal, transverse, and transverse interference response functions, respectively. The squared four-momentum transfer is given by $Q^2 = q^2 - \omega^2 = -q_\mu^2$. For the NC scattering, σ_M^Z is defined by

$$\sigma_M^Z = \left(\frac{G_F \cos(\theta_l/2) E_f M_Z^2}{\sqrt{2}\pi(Q^2 + M_Z^2)} \right), \quad (2)$$

where M_Z is the rest mass of the Z boson and G_F is the Fermi constant. The recoil factor f_{rec} is given as

$$f_{\text{rec}} = \frac{E_{A-1}}{M_A} \left| 1 + \frac{E_p}{E_{A-1}} \left[1 - \frac{\mathbf{q} \cdot \mathbf{p}}{p^2} \right] \right|. \quad (3)$$

For the NC reaction, the forms for the kinematical coefficients v and the corresponding response functions in Eq. (1) are given in Ref. [23].

The weak current J^μ represents the Fourier transform of the nucleon current density written as

$$J^\mu = \int \bar{\psi}_p \hat{\mathbf{J}}^\mu \psi_b e^{i\mathbf{q} \cdot \mathbf{r}} d^3r, \quad (4)$$

where $\hat{\mathbf{J}}^\mu$ is a free weak nucleon current operator, and ψ_p and ψ_b are wave functions of the knocked-out nucleon and the bound state nucleon, respectively. For a free nucleon of the NC reaction, the current operator comprises the weak vector and the axial vector form factors

$$\hat{\mathbf{J}}^\mu = F_1^V(Q^2) \gamma^\mu + F_2^V(Q^2) \frac{i}{2M_N} \sigma^{\mu\nu} q_\nu + G_A(Q^2) \gamma^\mu \gamma^5, \quad (5)$$

where M_N denotes the mass of the nucleon. The vector form factors for the proton (neutron), $F_i^{V,p(n)}(Q^2)$, are expressed as [17]

$$F_i^{V,p(n)}(Q^2) = \left(\frac{1}{2} - 2 \sin^2 \theta_W \right) F_i^{p(n)}(Q^2) - \frac{1}{2} F_i^{n(p)}(Q^2) - \frac{1}{2} F_i^s(Q^2), \quad (6)$$

where θ_W is the Weinberg angle given by $\sin^2 \theta_W = 0.2224$.

The strange vector form factors $F_i^s(Q^2)$ in Eq. (6) are usually given as a dipole form [29], independently of the

nucleon isospin,

$$F_1^s(Q^2) = \frac{F_1^s(0)Q^2}{(1+\tau)(1+Q^2/M_V^2)^2}, \quad (7)$$

$$F_2^s(Q^2) = \frac{F_2^s(0)}{(1+\tau)(1+Q^2/M_V^2)^2},$$

where $\tau = Q^2/(4M_N^2)$ and $M_V = 0.843$ GeV is the cutoff mass parameter usually adopted for nucleon electromagnetic form factors. $F_1^s(0)$ is defined as the squared strange radius of the nucleus, $F_1^s(0) = -\langle r^2 \rangle/6 = dG_E^s(Q^2)/dQ^2|_{Q^2=0} = 0.53$ GeV⁻², and $F_2^s(0) = \mu_s = -0.4$ is an anomalous strange magnetic moment.

The axial form factors are given by [30]

$$G_A(Q^2) = \frac{1}{2}(\mp g_A + g_A^s)/(1+Q^2/M_A^2)^2, \quad (8)$$

where $g_A = 1.262$, $M_A = 1.032$ GeV, and $g_A^s = -0.19$, which represents the strange quark contents on the nucleon [31]. The $-(+)$ coming from the isospin dependence denotes the knocked-out proton (neutron). The g_A^s represents the strange quark contents in the nucleon.

Although the ambiguity from the strangeness in the nucleon still persists as discussed in our recent calculations regarding the parity violating electron scattering [32], we adopt the standard values because the contributions from the strangeness in the vector current are less than a few percent on relevant cross sections [33]. But the contribution by g_A^s , which is larger than that on the vector current, is still controversial even in the analysis of the MiniBooNE data. Therefore, we fixed g_A^s as -0.19 , which roughly corresponds to the BNL data [2].

III. RESULTS

Within the framework of a relativistic single-particle model, we investigate the effect stemming from the FSI between the knocked-out nucleon and the residual nucleus on the inclusive $\nu(\bar{\nu})$ -¹²C scattering via the NC reaction. The distorted wave functions of the knocked-out nucleons by the FSI are obtained by solving the Dirac equation under three different potentials: the phenomenological relativistic optical potential generated by EDAD1 [27] (labeled Opt.), the real part of the same optical potential (labeled real), and the same potential as the bound nucleons generated by TIMORA [28], referred to as RMF.

At first, in Fig. 1, we show how the FSI affects the differential cross sections in Eq. (1) for the ¹²C nucleus. Two different incident $\nu(\bar{\nu})$ energies, 500 MeV (left panels) and 1 GeV (right panels), are used. The upper and lower panels are the results for the incidents ν and $\bar{\nu}$, respectively. Solid (red) curves are the results obtained by using the RMF description of the FSI, dashed (black) curves were obtained by using the real part of the optical potential, dotted (blue) curves were obtained by using the optical potential including the imaginary part, and dash-dotted (sky blue) curves were calculated without the FSI, in which the plane wave of the knocked-out nucleons was used.

The effect of the FSI owing to the optical potential reduces the cross section by about a factor of 2 compared to that without the FSI, which is almost the same result as the inclusive (e, e')

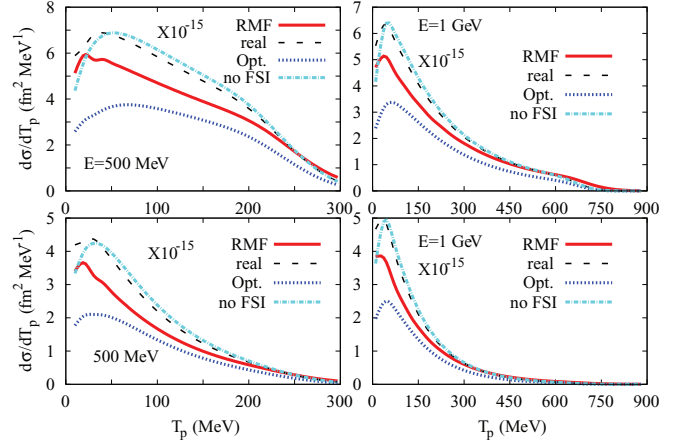


FIG. 1. (Color online) The effect of the FSI on the cross sections for ν -¹²C scattering in terms of the kinetic energy of the knocked-out nucleons for incident energies of 500 MeV and 1 GeV. The left (right) panels are for 500 MeV (1 GeV). The upper and the lower panels are the results for the incident neutrino and antineutrino, respectively. Solid (red) curves are the results for the RMF, dashed (black) curves are for the real term of optical potential, dotted (blue) curves are for the optical potential with including the imaginary term, and dash-dotted (sky blue) curves are without the FSI.

reaction. The effect of the RMF is the reduction of about 25% around the peak, while the effect of the real part of the optical potential enhances a little bit of the cross section before the peak position but the effect beyond the peak is a reduction of about 5%.

Therefore, the imaginary part of the optical potential which provides the information of strong absorption significantly suppresses the cross sections about 45%. These phenomena show up independently of both neutrino helicity and given kinematics. With the higher incident energies, the peak width becomes narrower. If we compare both cross sections by ν -A (upper) and $\bar{\nu}$ -A (lower), those of the ν -A are generally larger about 60% ~ 75% than those of the $\bar{\nu}$ -A because of the different helicity of $\bar{\nu}$.

Here we briefly discuss the three approaches for the inclusive ν -A scattering. For both NC and CC reactions, the incident neutrino energies cannot be measured but the knocked-out nucleons can be detected. In an aspect of kinematics, the difference between two reactions is whether the final leptons can be detected or not. For the NC reaction, the real potential is acceptable but the complex optical potential is not because the incident and the final neutrinos are not measured but the knocked-out nucleons can be detected. However, for the CC reaction, since both final leptons and knocked-out nucleons can be detected, the complex potential can be more adequate than the real potential but the real potential could be also a reasonable approach according to our previous paper [24].

In Figs. 2 and 3, we show the cross sections for protons and neutrons participating in the reaction, but detected separately. The kinematics are the same as Fig. 1. While the results in Fig. 1 are the summation of all nucleons participating in the reaction from a target nucleus, in Fig. 2, only protons in the target nucleus are taken into account in the reaction, and in Fig. 3 only neutrons are considered. By comparing Fig. 2 with

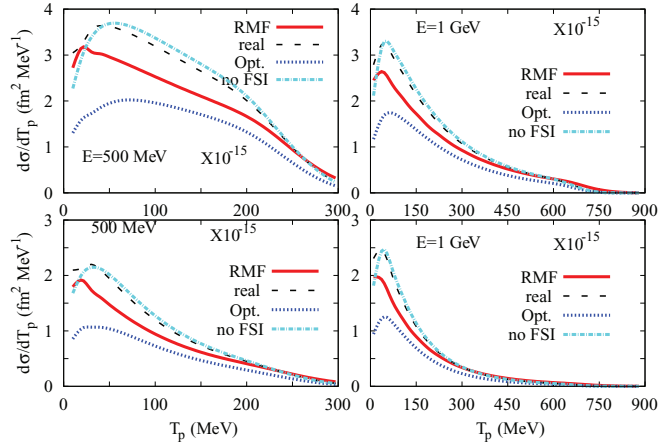


FIG. 2. (Color online) The same as Fig. 1, but for protons exclusively measured.

Fig. 3, whole features of the FSI effects in both cases are almost the same. It means that the FSI is nearly independent of the nucleon isospin, at least in the neutrino scattering on the QE region. But the magnitude of the cross sections on the protons is larger, about 10% maximally, than that on the neutrons for the incident neutrino and 1%~3% for the incident antineutrino. It means that the difference comes from the isospin effect of the weak form factor, which includes the vector and axial terms in Eqs. (6) and (8), which leads to the differences of the “no FSI” results between Figs. 2 and 3. Meucci *et al.* [17] calculated the effect of the FSI between a relativistic distorted wave impulse approximation and a relativistic plane wave impulse approximation. The FSI effect, which is given by the log scale and shows almost about 50% of corresponding cross sections, is in agreement with the difference between “no FSI” and “Opt.” in our results in Figs. 2 and 3.

In Fig. 4, detailed enumerations regarding the FSI effects on each separated response cross section are presented. At first, we investigate the FSI effects on the longitudinal cross sections which integrates the first term in Eq. (1) by the scattering angle (θ) and the polar angle (θ_p) of the knocked-out nucleon as

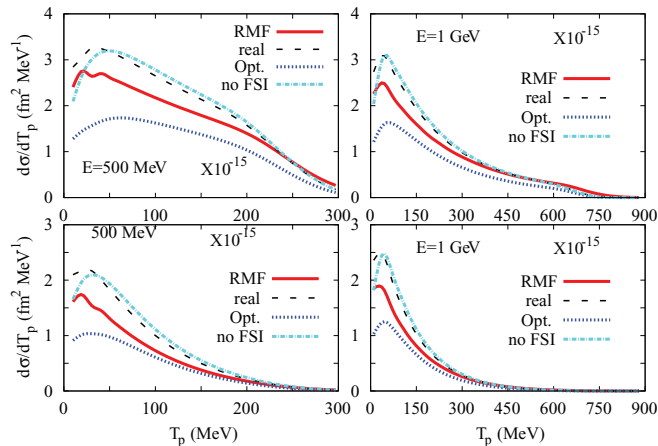


FIG. 3. (Color online) The same as Fig. 1, but for neutrons exclusively measured.

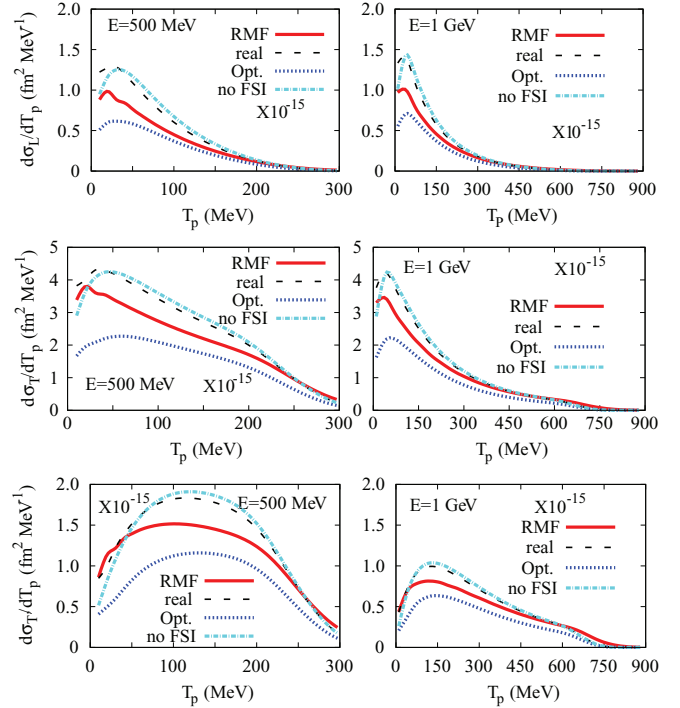


FIG. 4. (Color online) The FSI effects on longitudinal (first panel), transverse (second panel), and transverse interference (last panel) cross sections. The kinematics are the same as in Fig. 1.

shown in the first panel of Fig. 4. The kinematics are the same as Fig. 1. The FSI effects coming from the optical potential and its real potential are similar to those in Fig. 1. But the FSI effects by the RMF become larger than those on the entire cross sections in Fig. 1. In this case, the reduction is about 30% for 500 MeV and about 45% for 1 GeV around peak positions, while reduction of the entire cross section is about 25% in Fig. 1 (please note the scale difference between Figs. 1 and 4).

In the middle panels of Fig. 4, the FSI effects on the transverse cross sections are presented with the same kinematics as Fig. 1. Like the longitudinal cross sections, the FSI effects due to the optical potential and the real potential are similar to those in Fig. 1. But, in the case of the RMF description, the FSI effects are reduced about 15% for 500 MeV and about 20% for 1 GeV at peak. From these results, the FSI effects on the longitudinal (transverse) cross section by the RMF exhibit larger (smaller) effects than those on the cross sections.

The lower panels of Fig. 4 show the effects on the transverse interference cross sections, which are the last term in Eq. (1), with the same kinematics. The effects obtained by using the RMF and the real potential are similar to other cases. But the FSI effects obtained by using the optical potential are about 35% reduction. This means that the absorption in the interference term is not large in comparison with the about 45% in other terms.

One more point to be noticed in Fig. 4 is that shapes of the longitudinal and the transverse cross sections are similar to the corresponding cross sections. But, the magnitude on the transverse cross sections is as much as a factor of 3 in

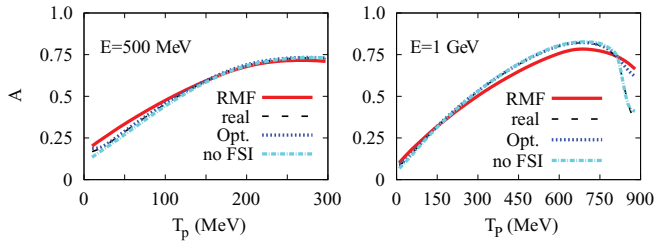


FIG. 5. (Color online) The FSI effects on the asymmetry between the ν -A and the $\bar{\nu}$ -A scattering. The kinematics are the same as in Fig. 1.

comparison with the longitudinal cross sections. This is an interesting result because, in the inclusive (e, e') reaction, the contribution of the longitudinal term is about 40%~50% at the forward scattering angle but at the backward angle is small [34]. On the other hand, the shape and the magnitude of the transverse interference cross sections are totally different from the other two response cross sections, which is also analogous to the electron scattering.

We also study the FSI effect on the asymmetry defined as

$$A = \frac{\sigma(h = -1) - \sigma(h = +1)}{\sigma(h = -1) + \sigma(h = +1)}, \quad (9)$$

where σ denotes the differential cross section in Eq. (1) and $h = -1(h = +1)$ represents the helicity of the incident $\nu(\bar{\nu})$. In Fig. 5, the FSI effects on the asymmetry are presented. The effects and the shapes of the FSI are fully different from those on the preceding cross sections. Namely, the FSI effects of the RMF around peak are about 3% at 500 MeV and 6% at 1 GeV maximally, but others are less than 1%. The effects of the FSI somewhat cancel each other out. Therefore, the measurement of the asymmetry could be an ideal way to study the ν -A scattering in the QE region, because it is almost independent of the FSI descriptions.

Furthermore, we calculate the ratios of the cross sections, to study which kinematical region is the most sensitive or insensitive to the FSI effects on the neutrino scattering in the QE region, as follows

$$R_i = \frac{\sigma_i}{\sigma_j}, \quad (10)$$

where σ_i denotes the cross section in Eq. (1) described by the RMF, the real potential, and the optical potential for the FSI and j denotes “no FSI” for the knocked-out nucleons.

Our results regarding the FSI sensitivity on the cross sections given by Eq. (10) are shown in Figs. 6 and 7. The upper panels are the results for the neutrino and the lower panels are for the antineutrino. Solid (red) curves represent the results for $i = \text{RMF}$, dashed (black) curves are for $i = \text{real potential}$, and dotted (blue) curves are for $i = \text{optical potential}$. The FSI effects on red curves are up to 30%, black curves are less than 10%, and blue curves are almost 50%. In particular, the ratios by all FSI descriptions show a rapid increase with the higher kinetic energies of the knocked-out nucleons. It means that one had better use the kinematical regions, $T_p = 75 \sim 150$ MeV for $E_\nu = 500$ MeV and $T_p = 150 \sim 450$ MeV for $E_\nu = 1$ GeV

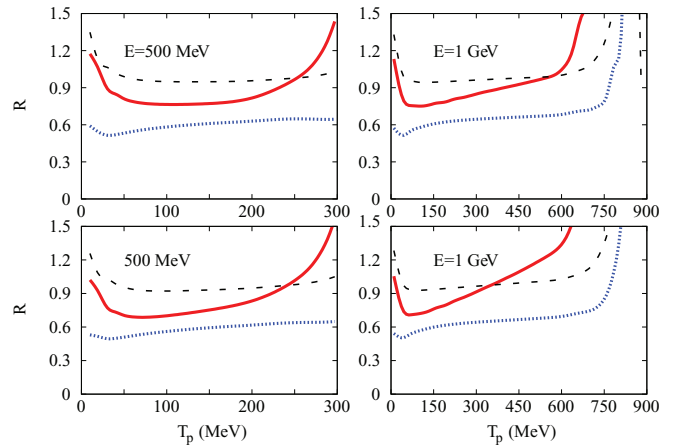


FIG. 6. (Color online) The cross section ratios, $R_i = \sigma_i/\sigma_j$, with $i = \text{the RMF, the real potential, and the optical potential}$ to the cross section without the FSI, σ_j . The upper (lower) panel is the results for the neutrino (the antineutrino). The detailed explanations of the curves are given in the text.

for less FSI dependence, whose energy regions correspond to the QE peak.

We show the FSI sensitivity on each response cross section, the longitudinal (upper), the transverse (middle), and the transverse interference (lower) cross sections in Fig. 7, whose ratios are calculated in the same manner as Eq. (10). The results are shown to be similar to those of whole cross sections in Fig. 6.

Finally, we calculate the flux-averaged differential cross section $\langle d\sigma/dQ^2 \rangle$ and compare our results with the Mini-BooNE data [9] in Fig. 8 by using the predicted ν_μ flux [3]. We present three different classes. One is to exploit a fictitious target proton H, another is ^{12}C , and the other is to use real CH_2

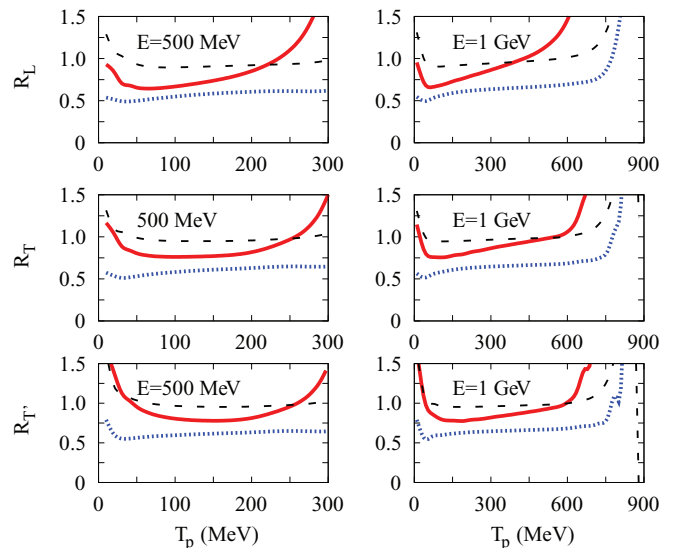


FIG. 7. (Color online) Same as Fig. 6 but for each response function.

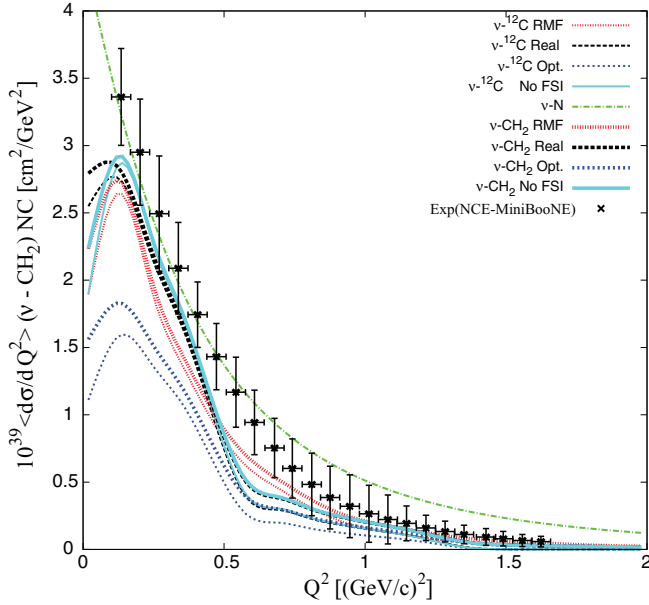


FIG. 8. (Color online) Flux-averaged differential cross sections $\langle d\sigma/dQ^2 \rangle$ per nucleon. The solid curve is the results for the No FSI, the dotted curve is for the optical potential, the dashed curve is for the real potential, and the short-dotted curve is for the RMF. Thin curves are the results only for the ^{12}C target and thick curves are for the CH_2 target including hydrogen. The experimental data are from the MiniBooNE experiment [9]. For a reference, results for ν - N are also presented as a dash-dotted (green) curve.

target, for which we use

$$\left\langle \frac{d\sigma}{dQ^2} \right\rangle = \frac{1}{7} \left\langle \frac{d\sigma_{\nu p \rightarrow \nu p, H}}{dQ^2} \right\rangle + \frac{3}{7} \left\langle \frac{d\sigma_{\nu p \rightarrow \nu p, C}}{dQ^2} \right\rangle + \frac{3}{7} \left\langle \frac{d\sigma_{\nu n \rightarrow \nu n, C}}{dQ^2} \right\rangle, \quad (11)$$

where we took the efficiency correction functions as unity. Our results are presented for each FSI description, i.e., results for RMF, Real, Opt., and No FSI are shown as short-dotted, dashed, dotted, and solid curves. For a reference, we show the cross section for ν - N scattering (dash-dotted curve) on the same kinematics, in which the cross section in the high Q^2 region is reduced strongly due to the inclusion of the ^{12}C ; that is, it reflects the nuclear medium effect. The results for the CH_2 target (thick curves) in each FSI description are about 10% larger than those for the ^{12}C target (thin curves) while the result for ν - N shows the largest cross section. Because cross sections are given per nucleon in each target, about a 10% increase by the CH_2 target and a greater increase by the proton target means the in-medium effects of the neutrino scattering off a nucleon inside the nuclear target.

If we compare our results to the experimental data, our results are smaller than the data by about 20%~30%, even if we take the CH_2 target, except the case of the optical potential which includes the imaginary part. This deficiency appears in any theoretical approaches. The effects of the FSI are of the same order as the previous results in Fig. 1. Note that we do not use new values of the axial mass (M_A) and the axial

strange form factor (g_A^s) obtained from the data [9], but use conventional values.

In the following we argue possible reasons for understanding the difference between our results and the data. (1) Multiparticle multihole contributions beyond 1p-1h turned out to be important for the CC reaction even in the QE region [35]. But those contributions are easily elusive in the NC reaction because of deficient knowledge of the kinematics by the nondetection of final neutrinos. Moreover, those contributions seem to be entangled with the FSI discussed here. (2) The second one is the change of axial mass and strangeness contents as done in the MiniBooNE analysis. In particular, the axial mass is increased to reproduce the CC and NC MiniBooNE data, even if we allow the strangeness content on the nucleon. But the value of the increased axial mass is not consistent with the value deduced from other experiments. More intensive discussions are necessary for this problem. (3) The third one is related to the neutrino flux deduced from the simulation of hadron scattering and its decays without considering oscillation by the presumed sterile neutrino. Recent data for the ν_μ and $\bar{\nu}_\mu$ disappearance in MiniBooNE and SciBooNE data [36,37] would give lots of indications for the discussion. (4) Final possible contributions are to come from inelastic channels, which are not considered in our calculation. More comprehensive coupled-channel approaches including elastic and inelastic channels are to be developed.

IV. SUMMARY AND CONCLUSION

In this work, we investigate the FSI effects on the differential cross sections for the inclusive $\nu(\bar{\nu})$ - ^{12}C scattering in the QE region with all bound nucleons, only protons, and only neutrons. Our numerical results show that the FSI effects in the inclusive scattering via NC play a vital role in the cross sections and the estimated FSI magnitudes are almost the same as the inclusive electron $^{12}\text{C}(e, e')$ scattering. In particular, the resultant FSI effects on the contribution to the knocked-out protons are larger than those of the neutrons by 10% for the incident neutrino and 1%~3% for the antineutrino. But, they come mainly from the nucleon isospin effect in the weak current.

The effects of the FSI are also examined separately for each longitudinal, transverse, and transverse interference cross section, which are integrated in terms of the scattering angle and the polar angle of the knocked-out nucleons in Eq. (1). For the longitudinal and the transverse cross sections, the FSI by the RMF description appears in a different way from the cross sections, while the FSI by the optical potential appears similar to the cross sections. But in the transverse interference cross sections, the FSI effect by the optical potential is reduced by comparing with other cases while the RMF is almost the same. The effects for the real part of the optical potential, which are not large, are same for the all cases. The shape of the transverse interference cross sections differs from that of the differential cross sections while that of the longitudinal and transverse cross sections resembles the differential cross sections.

However, on the asymmetry between ν and $\bar{\nu}$ scattering, the effects and their shapes of the FSI show behaviors different

from those on the cross sections. The asymmetry is nearly independent of the FSI description schemes because the FSI effects are somewhat canceled out by each other between the denominator and the numerator in Eq. (9). The ratios with the FSI to those without the FSI for the cross section and each response cross section are also presented for looking for the kinematical regions relatively insensitive to the FSI descriptions. But the ratios show that the difference coming from the different FSI description is unavoidable, at least 50%, even in the selected kinematical region, and all the FSI effects increase rapidly with higher kinetic energies of the knocked-out nucleon. In addition, we compare our results with the experimental data measured from the MiniBooNE [9] but our results are smaller than the data by 20%~30%, which is consistent with other calculations. Possible reasons for the underestimation, multi-nucleon effects, change of axial mass, overestimated neutrino

flux, and contributions from inelastic channels, are argued shortly.

In conclusion, the effect of the FSI on the neutrino-nucleus scattering cross sections appears to be almost the same as that on the inclusive electron (e, e') scattering cross sections. However the effects for the each response cross section and the asymmetry behave differently from those on the cross sections. In particular, the FSI effects on the asymmetry are shown to be nearly independent of the FSI descriptions.

ACKNOWLEDGMENTS

This work was supported by a 2011 Korea Aerospace University Faculty Research Grant and by the National Research Foundation of Korea (Grants No. 2012R1A1A2041974, No. 2012M7A1A2055605, and No. 2011-0015467).

-
- [1] O. Moreno, P. Sarriguren, E. Moya de Guerra, J. M. Udias, T. W. Donnelly, and I. Sick, *Nucl. Phys. A* **828**, 306 (2009).
 - [2] K. Abe *et al.*, *Phys. Rev. Lett.* **56**, 1107 (1986); L. A. Ahrens *et al.*, *Phys. Rev. D* **35**, 785 (1987).
 - [3] A. A. Aguilar-Arevalo *et al.* (MiniBooNE Collaboration), *Phys. Rev. D* **81**, 092005 (2010).
 - [4] K. Abe *et al.* (T2K Collaboration), *Phys. Rev. Lett.* **107**, 041801 (2011).
 - [5] P. Adamson *et al.* (MINOS Collaboration), *Phys. Rev. Lett.* **107**, 181802 (2011).
 - [6] K. Abe *et al.* (Double Chooz Collaboration), *Phys. Rev. Lett.* **108**, 131801 (2012).
 - [7] F. P. An *et al.*, *Phys. Rev. Lett.* **108**, 171803 (2012).
 - [8] J. K. Ahn *et al.* (RENO Collaboration), *Phys. Rev. Lett.* **108**, 191802 (2012).
 - [9] A. A. Aguilar-Arevalo *et al.* (MiniBooNE Collaboration), *Phys. Rev. D* **82**, 092005 (2010).
 - [10] J. E. Amaro, M. B. Barbaro, J. A. Caballero, T. W. Donnelly, and C. F. Williamson, *Phys. Lett. B* **696**, 151 (2011).
 - [11] M. Martini, M. Ericson, G. Chanfray, and J. Marteau, *Phys. Rev. C* **80**, 065501 (2009).
 - [12] J. Nieves, I. R. Simo, and M. J. Vicente Vacas, *Phys. Rev. C* **83**, 045501 (2011); J. Nieves, F. Sánchez, I. R. Simo, and M. J. Vicente Vacas, *Phys. Rev. D* **85**, 113008 (2012); J. Nieves, I. R. Simo, and M. J. Vicente Vacas, *Phys. Lett. B* **707**, 72 (2012).
 - [13] A. M. Ankowski, *Phys. Rev. C* **86**, 024616 (2012).
 - [14] A. V. Butkevich and D. Perevalov, *Phys. Rev. C* **84**, 015501 (2011).
 - [15] A. Meucci, C. Giusti, and F. D. Pacati, *Phys. Rev. D* **84**, 113003 (2011).
 - [16] R. González-Jiménez, M. V. Ivanov, M. B. Barbaro, J. A. Caballero, and J. M. Udias, *Phys. Lett. B* **718**, 1471 (2013).
 - [17] A. Meucci, C. Giusti, and F. D. Pacati, *Nucl. Phys. A* **739**, 277 (2004).
 - [18] J. Ryckebusch, D. Debruyne, P. Lava, S. Janssen, B. Van Overmeire, and T. Van Cauteren, *Nucl. Phys. A* **728**, 226 (2003).
 - [19] M. C. Martinez, P. Lava, N. Jachowicz, J. Ryckebusch, K. Vantournhout, and J. M. Udias, *Phys. Rev. C* **73**, 024607 (2006).
 - [20] A. Meucci, C. Giusti, and F. D. Pacati, *Nucl. Phys. A* **744**, 307 (2004).
 - [21] J. Nieves, M. Valverde, and M. J. Vicente Vacas, *Phys. Rev. C* **73**, 025504 (2006).
 - [22] T. Leitner, L. Alvarez-Ruso, and U. Mosel, *Phys. Rev. C* **74**, 065502 (2006).
 - [23] K. S. Kim, B. G. Yu, M. K. Cheoun, T. K. Choi, and M. T. Cheong, *J. Phys. G* **34**, 2643 (2007).
 - [24] K. S. Kim and M.-K. Cheoun, *Phys. Rev. C* **83**, 034607 (2011).
 - [25] K. S. Kim, L. E. Wright, Y. Jin, and D. W. Kosik, *Phys. Rev. C* **54**, 2515 (1996); K. S. Kim, L. E. Wright, and D. A. Resler, *ibid.* **64**, 044607 (2001); K. S. Kim and L. E. Wright, *ibid.* **67**, 054604 (2003);
 - [26] K. S. Kim and L. E. Wright, *Phys. Rev. C* **56**, 302 (1997); **60**, 067604 (1999); **68**, 027601 (2003).
 - [27] E. D. Cooper, S. Hama, B. C. Clark, and R. L. Mercer, *Phys. Rev. C* **47**, 297 (1993).
 - [28] C. J. Horowitz and B. D. Serot, *Nucl. Phys. A* **368**, 503 (1981).
 - [29] G. Garvey, E. Kolbe, K. Langanke, and S. Krewald, *Phys. Rev. C* **48**, 1919 (1993).
 - [30] M. J. Musolf and T. W. Donnelly, *Nucl. Phys. A* **546**, 509 (1992).
 - [31] V. Bernard, L. Elouadrhiri, and U.-G. Meissner, *J. Phys. G* **28**, R1 (2002).
 - [32] K. S. Kim and M.-K. Cheoun, *J. Phys. Soc. Jpn.* **82**, 024201 (2013).
 - [33] M.-K. Cheoun and K. S. Kim, *J. Phys. G* **35**, 065107 (2008).
 - [34] K. S. Kim and L. E. Wright, *Phys. Rev. C* **72**, 064607 (2005).
 - [35] M. Martini, M. Ericson, and G. Chanfray, *Phys. Rev. C* **84**, 055502 (2011).
 - [36] K. B. M. Mahn *et al.* (MiniBooNE and SciBooNE Collaborations), *Phys. Rev. D* **85**, 032007 (2012).
 - [37] G. Cheng *et al.* (MiniBooNE and SciBooNE Collaborations), *Phys. Rev. D* **86**, 052009 (2012).